Romanian Reports in Physics, Vol. 59, No. 2, P. 729–740, 2007

Dedicated to Prof. Dorin N. Poenaru's 70th Anniversary

SEARCH FOR POSSIBLE WAY OF PRODUCING SUPER-HEAVY ELEMENTS – DYNAMIC STUDY ON DAMPED REACTIONS OF ^{244}Pu+^{244}Pu, ^{238}U+^{238}U AND ^{197}Au+^{197}Au

ZHUXIA LI[1,2,3,4], XIZHEN WU[1,2], NING WANG[5]

[1] *China Institute of Atomic Energy, Beijing 102413, P.R. China*
E-mail: lizwux@ciae.ac.cn, lizwux9@.ciae.ac.cn
[2] *Nuclear Theory Center of National Laboratory of Heavy Ion Accelerator Lanzhou 730000, P.R. China*
[3] *Institute of Theoretical Physics, Chinese Academic of Science Beijing 100080, P.R. China*
Department of Physics, Tsinghua University, Beijing 100084, P.R. China
[5] *Institute for Theoretical Physics at Justus-Liebig-University, D-35392 Giessen, Germany*

(Received March 1, 2007)

Abstract. By using the improved Quantum Molecular Dynamics model, the ^{244}Pu+^{244}Pu, ^{238}U+^{238}U and ^{197}Au+^{197}Au reactions at the energy range of $E_{c.m.} = 800$ MeV to 2 000 MeV are studied. We find that the production probability of superheavy fragments(SHF) with $Z \geq 114$ is much higher for ^{244}Pu+^{244}Pu reaction compared with that of ^{238}U+^{238}U reaction and no product of SHF is found for the ^{197}Au+^{197}Au. The production probability of SHF is narrowly peaked in the dependence of incident energies. The decay mechanism of the composite system of projectile and target and the time scale of decay process are explored. The binding energies of superheavy fragments are found to be broadly distributed and their shapes turn out to be exotic form.

Key words: low and intermediate energy heavy-ion reactions, nuclear reaction models and methods.

1. INTRODUCTION

There are two approaches proposed for producing superheavy elements through accelerators. The approach of the complete fusion reaction is very

successful [1, 2] in producing SHEs. Since the 70's the elements from Z=107 to 118 were synthesized in the "cold fusion" reactions with lead and bismuth targets and in the "hot fusion" reactions with actinide targets. However, it is well known that further experimental extension of the region of superheavy fragments to the central area of superheavy "island" by means of the complete fusion reaction is limited by the number of available projectiles and targets, and also by the very low production cross section [1, 3]. In order to approach the center of superheavy "island", which is very neutron-rich radioactive ion beams will have to be utilized, but up to now the intensive radioactive ion beams are not available. An alternative pathway to the synthesis of superheavy elements is the strongly damped collision process between very heavy nuclei, for instance, ^{238}U+ ^{238}U. The strongly damped collisions between the ^{238}U+^{238}U and the ^{238}U+^{248}Cm at the energies near the Coulomb barrier were studied in the '70s and the early '80s for searching superheavy nuclei [4, 5, 6, 7, 8]. It was reported in Ref. [9] that for the ^{238}U+^{238}U at E=7.5 AMeV, the upper limit of the cross-section for producing superheavy elements was about 2×10^{-32} cm^2 for half lives between milliseconds and month by looking for spontaneous events from reaction products. In Ref. [10] the reaction of ^{238}U+^{248}Cm at 7.4 AMeV was studied and it was found that the cross sections for ^{100}Fm, ^{99}Es, and ^{98}Cf with target of ^{248}Cm are three to four orders of magnitude higher than with target of ^{238}U. It means that the strongly damped reaction with two nuclei heavier than uranium could be very beneficial for producing superheavy nuclei. The theoretical study about this approach was mainly carried out by diffusion model [7] and quantum fluctuations within the fragmentation theory [6] at the '70s and the early '80s. Only recently, the studies on this kind of reactions are renewed [11, 12]. In Ref. [11], the production probability of primary superheavy fragments depending on incident energies and combinations of projectile and target were studied within the improved quantum molecular dynamics model. Whereas in Ref. [12] the low energy collisions of the ^{238}U+^{238}U and the ^{232}Th+^{250}Cf et al. were studied within multi-dimensional Langevin equations, in which the mass and charge distributions of primary and survived fragments formed in the reactions were mainly concerned.

For microscopically understanding of the mechanism of low energy collisions between very heavy nuclei and searching for a possible way for the synthesis of superheavy nuclei the approach of strongly damped reactions should be studied more extensively and thoroughly. In this work, we study the reactions of ^{244}Pu+^{244}Pu, ^{238}U+^{238}U and ^{197}Au+^{197}Au at the energy range of $E_{c.m.}$ = 800 MeV–2 000 MeV by the microscopically dynamical model. We concentrate on: 1) the energy-dependence of the production probability of superheavy fragments (SHFs) (Here, SHFs are defined as the fragments with

charge larger than or equal to 114), 2) the decay mechanism of the composite system of projectile and target, and 3) the distribution of binding energies and shapes of SHFs. Those studies can certainly provide us with very useful information about the mechanism of strongly damped reactions between very heavy nuclei and help us to search for a possible way for the synthesis of superheavy nuclei. Furthermore, they are also of a great significance for discovery of spontaneous positron emission from super-strong electric field by a static QED process [13] (transition from neutral to charged QED vacuum). The paper is organized as follows. In Section 2, we give a brief introduction of the improved quantum molecular dynamics model. The results of applications of this model to strongly damped reactions are reported in Section 3. Finally, the summary is given in Section 4.

2. THE ImQMD MODEL

In the Improved Quantum Molecular Dynamics (ImQMD) model, each nucleon is represented by a coherent state of a Gaussian wave packet [14, 15],

$$\phi_i(\mathbf{r}) = \frac{1}{(2\pi\sigma_r^2)^{3/4}} \exp\left[-\frac{(\mathbf{r}-\mathbf{r}_i)^2}{4\sigma_r^2} + \frac{i}{\hbar}\mathbf{r}\cdot\mathbf{p}_i\right], \tag{1}$$

where, $\mathbf{r}_i, \mathbf{p}_i$, are the center of i-th wave packet in the coordinate and momentum space, respectively. σ_r represents the spatial spread of the wave packet. Through a Wigner transformation, the one-body phase space distribution function for N-distinguishable particles is given by:

$$f(\mathbf{r},\mathbf{p}) = \sum_i \frac{1}{(\pi\hbar)^3} \exp\left[-\frac{(\mathbf{r}-\mathbf{r}_i)^2}{2\sigma_r^2} - \frac{2\sigma_r^2}{\hbar^2}(\mathbf{p}-\mathbf{p}_i)^2\right]. \tag{2}$$

The density and momentum distribution functions of a system read

$$\rho(\mathbf{r}) = \int f(\mathbf{r},\mathbf{p})d\mathbf{p} = \sum_i \rho_i(\mathbf{r}), \tag{3}$$

$$g(\mathbf{p}) = \int f(\mathbf{r},\mathbf{p})d\mathbf{r} = \sum_i g_i(\mathbf{p}), \tag{4}$$

respectively, where the sum runs over all particles in the system. $\rho_i(\mathbf{r})$ and $g_i(\mathbf{p})$ are the density and momentum distributions of nucleon i:

$$\rho_i(\mathbf{r}) = \frac{1}{(2\pi\sigma_r^2)^{3/2}} \exp\left[-\frac{(\mathbf{r}-\mathbf{r}_i)^2}{2\sigma_r^2}\right], \tag{5}$$

$$g_i(\mathbf{p}) = \frac{1}{(2\pi\sigma_p^2)^{3/2}} \exp\left[-\frac{(\mathbf{p}-\mathbf{p}_i)^2}{2\sigma_p^2}\right], \tag{6}$$

where σ_r and σ_p are the widths of wave packets in coordinate and momentum space, respectively, and they satisfy the minimum uncertainty relation:

$$\sigma_r \sigma_p = \frac{\hbar}{2}. \tag{7}$$

The propagation of nucleons under the self-consistently generated mean field is governed by Hamiltonian equations of motion:

$$\dot{\mathbf{r}}_i = \frac{\partial H}{\partial \mathbf{p}_i}, \quad \dot{\mathbf{p}}_i = -\frac{\partial H}{\partial \mathbf{r}_i}. \tag{8}$$

Hamiltonian H consists of the kinetic energy and effective interaction potential energy,

$$H = T + U, \tag{9}$$

$$T = \sum_i \frac{\mathbf{p}_i^2}{2m}. \tag{10}$$

The effective interaction potential energy includes the nuclear local interaction potential energy and Coulomb interaction potential energy,

$$U = U_{loc} + U_{Coul}, \tag{11}$$

and

$$U_{loc} = \int V_{loc}(\mathbf{r}) d\mathbf{r}, \tag{12}$$

where $V_{loc}(\mathbf{r})$ is potential energy density.

In the ImQMD model, the effective local interaction is introduced according to Skyrme interaction energy density functional

$$V_{loc} = \frac{\alpha}{2}\frac{\rho^2}{\rho_0} + \frac{\beta}{\gamma+1}\frac{\rho^{\gamma+1}}{\rho_0^{\gamma}} + \frac{g_{sur}}{2\rho_0}(\nabla\rho)^2 + \frac{C_s}{2\rho_0}(\rho^2 - \kappa_s(\nabla\rho)^2)\delta^2 + g_\tau \frac{\rho^{\eta+1}}{\rho_0^{\eta}}. \tag{13}$$

Here, $\delta = (\rho_n - \rho_p)/(\rho_n + \rho_p)$ is the isospin asymmetry and the ρ, ρ_n, ρ_p are the nucleon, neutron, and proton density, respectively. The first three terms in above expression can be obtained from the potential energy functional of Skyrme force directly. The fourth term is the symmetry potential energy where both the bulk and the surface symmetry potential energy are included. The surface symmetry potential energy term modifies the symmetry potential at the surface region and it is important for having a correct neutron skin and neck dynamics in heavy ion collisions. The last term in the potential energy functional is a small correction term. From the integration of V_{loc}, we obtain

the local interaction potential energy:

$$U_{loc} = \frac{\alpha}{2}\sum_i\sum_{j\neq i}\frac{\rho_{ij}}{\rho_0} + \frac{\beta}{\gamma+1}\sum_i\left(\sum_{j\neq i}\frac{\rho_{ij}}{\rho_0}\right)^{\gamma} + \frac{g_0}{2}\sum_i\sum_{j\neq i}f_{sij}\frac{\rho_{ij}}{\rho_0} + g_\tau\sum_i\left(\sum_{j\neq i}\frac{\rho_{ij}}{\rho_0}\right)^{\eta} + \frac{C_s}{2}\sum_i\sum_{j\neq i}t_it_j\frac{\rho_{ij}}{\rho_0}\left(1-\kappa_s f_{sij}\right), \quad (14)$$

where

$$\rho_{ij} = \frac{1}{(4\pi\sigma_r^2)^{3/2}}\exp\left[-\frac{(\mathbf{r}_i-\mathbf{r}_j)^2}{4\sigma_r^2}\right], \quad (15)$$

$$f_{sij} = \frac{3}{2\sigma_r^2} - \left(\frac{\mathbf{r}_i-\mathbf{r}_j}{2\sigma_r^2}\right)^2, \quad (16)$$

and t_i=1 and −1 for proton and neutron, respectively.

The Coulomb energy can be written as the sum of the direct and the exchange contribution

$$U_{Coul} = \frac{1}{2}\int\int\rho_p(\mathbf{r})\frac{e^2}{|\mathbf{r}-\mathbf{r}'|}\rho_p(\mathbf{r}')d\mathbf{r}d\mathbf{r}' - e^2\frac{3}{4}\left(\frac{3}{\pi}\right)^{1/3}\int\rho_p^{4/3}d\mathbf{R}, \quad (17)$$

where ρ_p is the density distribution of protons of system. The collision term and phase space occupation constraint can also readjust the momenta, but the former plays a very small role in low energy heavy ion collisions and the latter only happens occasionally. The phase space occupation constraint method [16] and the system-size-dependent initial wave-packet width [17] $\sigma_r = c_0 + c_1 N^{1/3}$ are adopted as in the previous version of the ImQMD [17, 18].

3. **RESULTS**

The parameters used in the calculation is given in Table 1. With this set of parameters we have checked that the properties of nuclear ground state, such as the binding energies and the root mean square radii, and the fusion

Table 1

The IQ2 model parameters

α MeV	β MeV	γ	g_0 MeVfm^2	g_τ MeV	η	C_s MeV	κ_s fm^2	ρ_0 fm^{-3}	c_0 fm	c_1 fm
-356	303	7/6	7.0	12.5	2/3	32.0	0.08	0.165	0.88	0.09

(capture) cross sections of light and intermediate heavy nuclei (heavy nuclei) can be described well. For strongly damped reaction of the ^{197}Au+^{197}Au at 35 AMeV under central collisions, the charge distribution of products has been calculated and compared with experimental data [19], as shown in Fig. 1. We find that the agreement is quite satisfied.

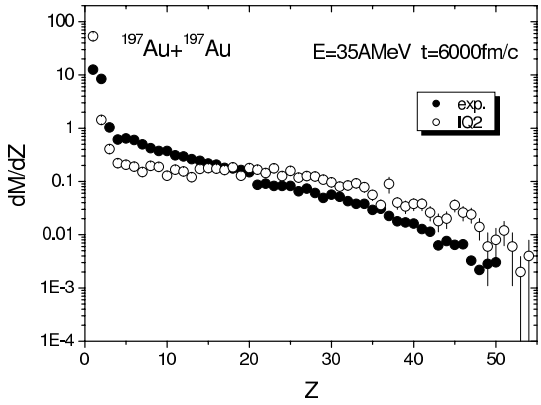

Fig. 1 – The charge distribution of the central collisions of ^{197}Au+^{197}Au at 35 AMeV. The simulation ends at 6 000 fm/c. The open and solid circles denote the calculated results and experimental data [19], respectively.

Now let us apply the ImQMD model to study strongly damped reactions of ^{244}Pu+^{244}Pu and ^{238}U+^{238}U at energy range of $E_{c.m.}$ = 800 MeV–2 000 MeV. The impact parameters are taken to be 1 fm and 3 fm. The initial nuclei of projectile and target are prepared by the same procedure as that in Ref. [17] and [18]. Fig. 2 shows the energy dependence of the production probability of SHFs for reactions of ^{244}Pu+^{244}Pu, ^{238}U+^{238}U and ^{197}Au+^{197}Au at impact parameter b = 1 fm. One pronounced feature obtained from Fig. 2 is strong dependence of the production probability of SHFs on the reaction systems. The production probability of ^{244}Pu+^{244}Pu is the highest, and that of the ^{238}U+^{238}U is only half of the Pu+Pu's yield. For the ^{197}Au+^{197}Au, the production probability of SHFs is about zero in the present calculations. The another pronounced feature is the narrowly peaked energy dependence of the production probability of SHFs. The location of the peak is at about $E_{c.m.}$ = 1 000 MeV for the ^{244}Pu+^{244}Pu and at $E_{c.m.}$ = 950 MeV for the ^{238}U+^{238}U. Although the location of peak energy may not be precise enough in this primary calculation, such behavior of the energy dependence of the production probability of SHFs should be correct. The narrowly peaked energy dependence means that it is crucial to select the correct incident energy in order to search superheavy elements experimentally by using this approach. We notice that the energies used in the experiments done [9, 8, 10] in the '70s

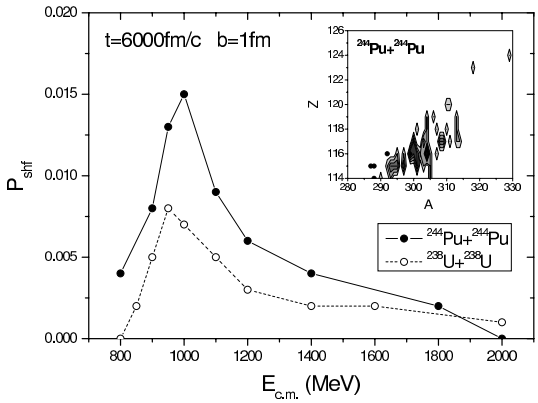

Fig. 2 – The incident energy dependence of the production probability of superheavy fragments with $Z \geq 114$ in reactions of ^{244}Pu+^{244}Pu and ^{238}U+^{238}U with impact parameter $b = 1$ fm. The inserted figure is the contour plot of mass and charge distributions of the products with Z $\geq$ 114 at the time $t = 6\,000$ fm/c for the reaction of ^{244}Pu+^{244}Pu, in which the solid circles denote the experimental data of isotopes of ^{288}114, ^{287,288}115 and ^{292}116 [2].

and '80s for the reaction of ^{238}U+^{238}U are lower than the peak energy given in this work. The production probability of SHFs corresponding to the energies used in [9, 8, 10] is much lower than that at the peak energy. The behavior of the incident energy dependence of the production probability of SHFs at impact parameter $b = 3$ fm is quite similar with at $b = 1$ fm. In the inserted figure of Fig. 3 the contour plot of mass and charge distributions of SHFs for the reaction of ^{244}Pu+^{244}Pu at the time $t = 6\,000$ fm/c is shown. For comparison, the experimental data of isotopes of ^{288}114, ^{287,288}115 and ^{292}116 [2] are also given in the figure by the black points. One can see from the figure that quite a few SHFs in the reaction of Pu+Pu are very neutron-rich and the corresponding neutron-to-proton ratio is much higher than that of experimentally produced ^{288}114, ^{287,288}115 and ^{292}116 . This character seems to be very useful for approaching to the center of superheavy "island".

Now let us discuss the decay mechanism of the composite system of projectile and target. Fig. 3 shows the time evolution of the number of SHFs for the reaction of ^{244}Pu+^{244}Pu at $E_{c.m.} = 1\,000$ MeV and the ^{238}U+^{238}U at $E_{c.m.} = 950$ MeV with impact parameters $b = 1, 3$ fm. The number of SHFs for each impact parameter given in Fig. 3 is obtained within 1 000 events.

From Fig. 3 two stages of the decay process of the composite systems can be distinguished by different decreasing slope, which implies different decay mechanism of the composite system. From 1 000 fm/c to 1 500 fm/c, the number of giant composite systems including SHFs decreases quickly with time increasing. During this stage called the first decay, the composite system

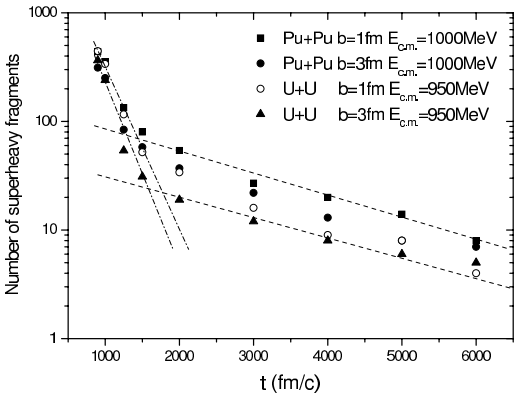

Fig. 3 – The time evolution of the number of fragments with $Z \geq 114$ including the heavy residues of composite systems for the reaction of ^{244}Pu+^{244}Pu at $E_{c.m.} = 1\,000$ MeV and $b = 1$ and 3 fm, and for the reaction of ^{238}U+^{238}U at $E_{c.m.} = 950$ MeV and $b = 1$ and 3 fm from time $t = 1\,000$ to $6\,000$ fm/c.

is firstly broken up into two pieces. In most of cases, the composite system is broken up into two pieces with size close to the initial nuclei. In a few cases it is broken up into two pieces with one heavier fragment and another smaller fragment, among which there exists possibility of producing one SHF and another one with $Z \sim 70$. In this stage we have counted the number of the existing composite systems at different time. At $t = 1\,000$ fm/c, more than 60 percent of events are still in the stage of two reaction partners sticking together, then at 1 200 fm/c, about 10–15 percent of events remain in this stage, and at 1 500 fm/c only few event remains in this stage, i.e. for almost all events, the composite system has been broken up into two pieces. In the second decay stage which appears after 1 500 fm/c, the products from the first decay including SHFs decreases slowly with time. In this stage, the SHFs decrease through emitting neutron, proton or other charged particles, and also through fission.

Now let us give a schematic description of the dynamical process of the strongly damped reaction of ^{244}Pu+^{244}Pu and ^{238}U+^{238}U. Fig. 4 shows the schematic diagram for the process of the reaction ^{244}Pu+^{244}Pu. When two reaction partners approach together a composite system of di-nuclei is transiently created. At about 1 000 fm/c the composite system breaks. About 70 percent of the composite systems are broken up into two pieces with mass around ^{244}Pu and the left 30 percent are broken into non-equal size two pieces in which the larger one probably belongs to SHFs. Then this larger piece including SHFs will further undergo being broken up into two pieces which happens at about 1 500 fm/c or surviving. The eventually survived SHFs will decay by emitting nucleons and light particles.

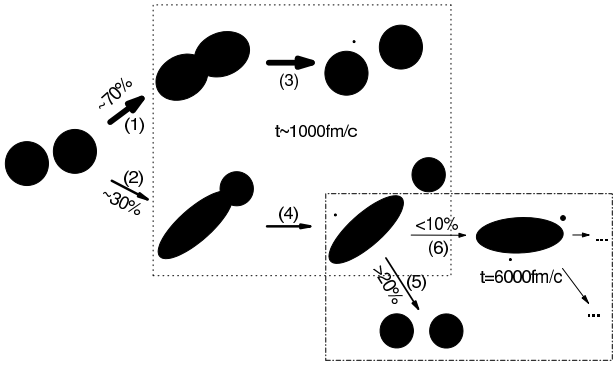

Fig. 4 – The schematic figure for the dynamical processes of the strongly damped reaction of ^{244}Pu+^{244}Pu.

Now we turn to study the configuration and structure of produced SHFs. We find that the primary superheavy fragments may manifest very exotic forms, such as the band-like or toroidal configuration. In Fig. 5 we illustrate the shapes of typical SHFs in the reaction of ^{244}Pu+^{244}Pu at $t = 6\,000$ fm/c

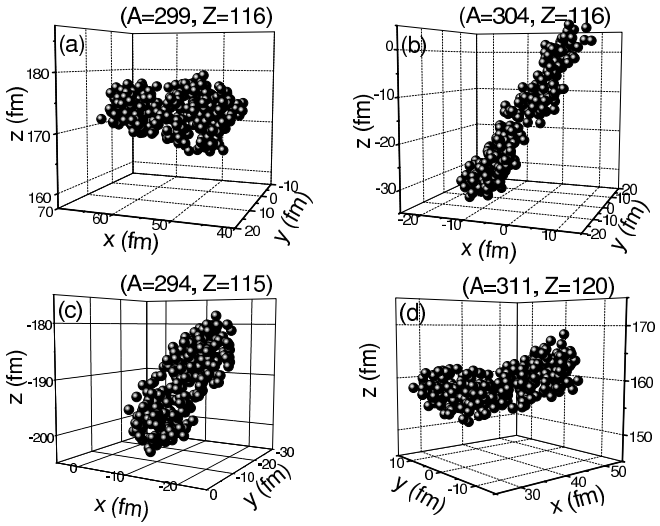

Fig. 5 – The structure and configuration of four typical superheavy fragments in the reaction of Pu+Pu at $E_{c.m.} = 1\,000$ MeV and $t = 6\,000$ fm/c with $b = 1$ fm.

and $E_{c.m.} = 1\,000$ MeV with the impact parameter $b = 1$ fm. The figure is drawn in the central mass frame and the beam direction is along the Z axis. Each of subfigures corresponds to the different SHF, which demonstrates the different structure and shape. The common characteristic of the structure is a

large elongation with some "bubbles". Our dynamical calculation shows that this kind of structure can keep stable at least for 5 000 fm/c.

In Fig. 6 we show the distributions of (a) the binding energies and (b) the R_z/R_ρ ratios of SHFs produced in the reaction of ^{244}Pu+^{244}Pu at

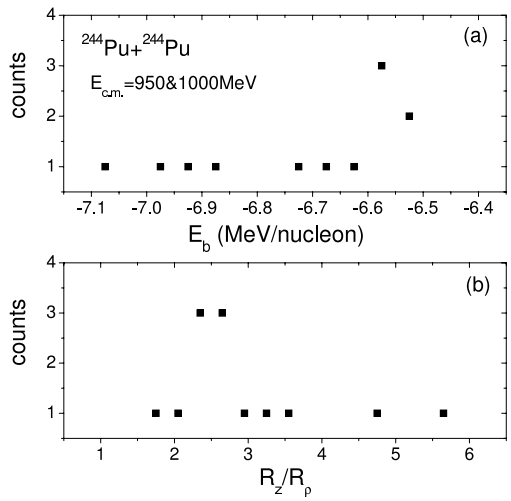

Fig. 6 – The distributions of: a) the binding energies; b) the $R_z/R\rho$ ratio of SHFs produced in the reaction of ^{244}Pu+^{244}Pu at $E_{c.m.} = 1\,000$ MeV and 950 MeV with $b = 1$ fm.

$E_{c.m.} = 1\,000$ MeV and 950 MeV with $b = 1$ fm. The R_z is the long axis and R_ρ is the short axis of SHF. The figure gives the counting numbers of SHFs in 1 000 reaction events versus (a) the binding energies and (b) the values of R_z/R_ρ. From Fig. 6(a) one sees that the binding energies of SHFs are broadly distributed. In the large binding energy side, the binding energy reaches about 7 MeV/nucleon, which is not far from the value of the predicted binding energy of the ground state of corresponding superheavy elements. The feature of broad distribution of binding energies of SHFs tailing to large binding energy is favorable to have larger surviving probability of SHF. From Fig. 6(b) one sees that the SHFs are strongly deformed. In most of the cases, they are at about super-deformation or even hyper-deformation. For those SHFs with super-deformed shape it is found that there are some bubbles in the density distribution (bubble-like). However, there also exist some SHFs with exotic shapes with $R_z/R_\rho \geq 4$. The shape of these SHFs is band-like. It is very surprising that the shape of SHFs has such exotic form. Such exotic forms of SHFs may be attributed to the huge electric charge. Associating the recent structure studies of superheavy nuclei within the RMF and HFB theory [20, 21, 22] in which very large deformed isomeric states were predicted, the

exotic form of SHFs seems to be understandable. However, the subject of exotic (bubble,band-like) configurations in super-heavy elements in which the interplay between Coulomb interaction and nuclear interaction becomes very important needs to be further studied.

4. SUMMARY

We have studied the strongly damped reactions of ^{244}Pu+^{244}Pu, ^{238}U+^{238}U and ^{197}Au+^{197}Au by using the ImQMD model. It is found that the production probability of SHFs strongly depends on the reaction systems and the incident energies. The production probability of SHFs in the ^{244}Pu+^{244}Pu reaction is much higher than that in the ^{238}U+^{238}U reaction, and no production of SHF has been found for the ^{197}Au+^{197}Au reaction in the present study. The incident energy dependence of the production probability of SHFs is narrowly peaked. The peak energy also depends on the reaction system. Thus, the suitable selection of the incident energy is very important in experimentally searching super-heavy elements by means of strongly damped massive nuclear reactions. The decay process of the giant composite system can be divided into two stages. The first one is a fast process by breaking the composite system into two pieces. In most cases the composite system is broken up into two pieces with sizes close to initial nuclei. Occasionally, it becomes into one superheavy fragment which will further be broken up into two pieces and a small piece as well. The second stage is a slow process with emitting light charged particles and nucleons as well as further breaking of SHFs. The binding energies of produced SHFs are distributed broadly. Its tail at large binding energy side is not far from the predicted binding energy of the corresponding SHE and therefore is favorable to producing superheavy elements. The primary superheavy fragments may manifest very exotic forms, such as the band-like or toroidal. In most of the cases, they are at about super-deformation or even hyper-deformation with some bubble in density distribution. This study certainly is very preliminary, there still a lot of works should be done.

Acknowledgements. This paper is supported by the National Natural Science Foundation of China under Grant Nos. 10235030, 10235020 and by Alexander von Humboldt Foundation.

REFERENCES

1. S. Hofmann and G. Münzenberg, Rev. Mod. Phys., **72**, 733 (2000).

2. Yu.Ts. Oganessian *et al.*, Phys. Rev., **C 63**, 011301(R) (2001); Phys. Rev., **C 69**, 021601(R) (2004).
3. Yu.Ts. Oganessian *et al.*, Eur. Phys. J. A., **13**, 135 (2002); **15**, 201 (2002).
4. Günter Herrmann, Nature, **280**, 543 (1979).
5. G.T. Seaborg, W. Loveland and D.J. Morrissey, Scince, **203**, 711 (1979).
6. J.A. Maruhn, J. Hahn, H.-J. Lustig, K.-H. Ziegenhan and W. Greiner, *Progress in Particle and Nuclear Physics*, Vol. 4, 257–271 (1980).
7. C. Riedel and W. Nörenberg, Z. Phys., **290**, 385 (1979).
8. H. Gäggeler, N. Trautmann, W. Brüchle *et al.*, Phys. Rev. Lett., **45**, 1824 (1980).
9. K.D. Hildenbrand, H. Freiesleben, F. Pühlhofer *et al.*, Phys. Rev. Lett., **39**, 1065 (1977).
10. M. Schädel, J.V. Kratz, H. Ahrens *et al.*, Phys. Rev. Lett., **41**, 469 (1978); M. Schädel, W. Brüchle, H. Gäggeler *et al.*, Phys. Rev. Lett., **48**, 852 (1982).
11. N. Wang, Z.X. Li, X.Z. Wu *et al.*, Mor. Phys. Lett., **A 20**, 1 (2005).
12. V.I. Zagrebaev, Yu.Ts. Oganessian, M.G. Itkis, and W. Greiner, Phys. Rev., **C 73**, 031602(R) (2006).
13. W. Greiner (Editor),*Quantum Electrodynamics of Strong Fields*, Plenum Press, New York, London, 1983.
14. Ch. Hartnack, Zhuxia Li, L. Neise *et al.*, Nucl. Phys., **A 495**, 303 (1989); Zhuxia Li, Ch. Hartnack, H. Stoecker and W. Greiner, Phys. Rev., **C 40**, 824 (1991).
15. J.Aichelin, Phys. Rep., **202**, 233 (1991), and references therein.
16. M. Papa, T. Maruyama, and A. Bonasera, Phys. Rev., **C 64**, 024612 (2001).
17. Ning Wang, Zhuxia Li, Xizhen Wu, Phys. Rev., **C 65**, 064608 (2002).
18. Ning Wang, Zhuxia Li, Xizhen Wu *et al.*, Phys. Rev., **C 69**, 034608 (2004).
19. P. Dsesquelles, M. D'Agostino *et al.*, Nucl. Phys., **A 633**, 547 (1998).
20. M. Bender, W. Nazarewicz, and P.G. Reinhard, Phys. Lett., **B 515**, 42 (2001).
21. F.R. Xu, E.G. Zhao, R. Wyss *et al.*, Phys. Rev. Lett., **92**, 252501 (2004).
22. Zhongzhou Ren, Phys. Rev., **C 65**, 051304 (R) (2002).